One-Way Ramp to a Two-Way Highway

Negar Reiskarimian, Tolga Dinc, Jin Zhou, Tingjun Chen, Mahmood Baraani Dastjerdi, Jelena Diakonikolas, Gil Zussman, and Harish Krishnaswamy

Since the invention of the radio, transmission and reception have been separated to protect the receiver (Rx) from being jammed by self-interference (SI), i.e., the interference that comes from the colocated radio transmitter (Tx). This separation is called *duplexing*. Today's wireless systems still rely on duplexing to avoid SI—many short-range or local area radios, such as Bluetooth and WiFi transceivers, transmit and receive in nonoverlapping time slots, called *time-division duplexing* (*TDD*), while other modern wireless systems, such as the majority of today's cellular systems, use frequency-division duplexing (FDD) to separate the transmission and reception in the frequency domain. Both TDD and FDD are half duplex, where the separation of the transmitted and received signals of a single user in either frequency or time causes inefficient utilization of limited wireless resources.

Full-duplex (FD) wireless, an emerging wireless communications paradigm, allows simultaneous transmission and reception at the same frequency, promising a significant enhancement in spectral efficiency at the physical layer. This results in many other benefits at the wireless network level, such as achieving better spectral efficiency, reducing network and feedback signaling delays, and resolving hidden-node problems to

Negar Reiskarimian (nr2475@columbia.edu), Tingjun Chen (tingjun@ee.columbia.edu), Mahmood Baraani Dastjerdi (mb4038@columbia.edu), Gil Zussman (gil@ee.columbia.edu), and Harish Krishnaswamy (harish@ee.columbia.edu) are with Columbia University, New York, United States. Tolga Dinc (t-dinc@ti.com) is with Texas Instruments, Dallas, United States. Jin Zhou (jinzhou@illinois.edu) is with University of Illinois Urbana-Champaign, United States. Jelena Diakonikolas (jelena.d@berkeley.edu) is with the University of California Berkeley, United States.

Digital Object Identifier 10.1109/MMM.2018.2880497

Date of publication: 11 January 2019

avoid collisions [1]–[5]. Additionally, FD systems based on a shared-antenna interface are crucial for enabling FD capability in handheld devices [6] as well as to extend the concept to multiple-input, multiple-output (MIMO) applications, such as FD massive MIMO base stations to reduce the overhead of channel state information (CSI) estimation [7], [8].

The biggest challenge associated with FD wireless, however, is the tremendous amount of SI on top of the desired signal. For example, given +20-dBm Tx output power, 15-dB isolation at the antenna interface, 20-MHz Rx signal bandwidth (BW), and a 5-dB Rx noise figure (NF), the SI at the Rx input is more than ten billion times stronger than the Rx noise floor.

Recent demonstrations leveraging commodity software-defined radios and/or off-the-shelf components (such as [2] and [9]–[13]) have established the feasibility of FD wireless through SI suppression at the antenna interface and SI cancellation (SIC) in the analog/RF and digital domains. Thanks to advances in complementary metal oxide semiconductor integrated circuits (CMOS IC) technology, complex digital SIC algorithms that offer approximately 50-dB SIC can be readily implemented. However, the analog/RF SIC in many existing FD demonstrations relies on cancellers that use bulky off-the-shelf components that do not readily translate to compact and low-cost IC implementations.

Performing analog/RF SIC in an IC is critical to bring FD wireless technology to mobile devices, such as handsets and tablets [14]–[25]. This article reviews the challenges associated with integrated FD radios and networks and briefly covers recent research at Columbia University and elsewhere on integrated analog/RF SIC. It also touches upon the Full-Duplex Wireless: From Integrated Circuits to Networks (FlexICoN) project at Columbia, which examines the cross-layer codesign of the physical layer and the network layer for FD wireless, including the development of FD testbeds to experimentally evaluate FD systems based on realistic hardware. One of the remaining open challenges for small-form-factor FD radios (perhaps the most important one) is the implementation of a low-loss shared-antenna interface with high Tx-to-Rx isolation for FD wireless. Shared-antenna interfaces enable compact form factor, translate easily to MIMO, and ease system design through channel reciprocity. The bulk of this article will review some of the recent research advances at Columbia University on integrated FD nonmagnetic CMOS circulators and antennas for simultaneous-transmit-and-receive (STAR) radios [18]–[20], [26], [27].

FD Challenges and an Overview of Columbia's FlexICoN Project

In this section, we present a brief discussion of the challenges associated with integrated FD radios and networks as well as an overview of recent research efforts to address them. We also provide an overview of the Full-Duplex Wireless: From Integrated Circuits to Networks (FlexICoN) project initiated at Columbia.

Compact FD Antenna Interfaces

An ideal antenna interface for FD should be compact, have no loss, and provide extremely high-power handling without any additional power consumption. Most existing FD demonstrations rely on bulky off-the-shelf antenna interfaces (such as antenna pairs and nonreciprocal ferrite circulators), which are not applicable to form-factor-constrained mobile applications where compact integrated FD antenna interfaces are desired. Compact FD antenna interfaces are also more compatible with MIMO and diversity applications. Furthermore, single-antenna FD ensures wireless channel reciprocity, which is useful at the higher layers. (Wireless channel reciprocity should not be confused with the nonreciprocity required to implement circulators. *Wireless channel reciprocity* refers to the fact that the wireless channel between two nodes is the same irrespective of which node is transmitting and which node is receiving.) Traditionally, nonreciprocal circulators have been implemented using ferrite materials that exhibit nonreciprocity via the Faraday effect in the presence of an external magnetic field. Since ferrite materials are incompatible with IC fabrication processes, ferrite circulators are expensive and bulky. Therefore, novel techniques that enable high-performance nonmagnetic integrated circulators are of high interest.

Another proposed reciprocal shared-antenna interface for FD is the electrical-balance duplexer (EBD), a hybrid transformer that is able to provide isolation between the Tx and the Rx through a balancing impedance at the expense of a minimum of 3-dB loss between the Tx and the antenna and between the antenna and the Rx [14], [28]–[31]. Additionally, [14], [24], and [32] have shown compact single-antenna polarization-duplexing STAR radios using orthogonal polarizations for the Tx and Rx. Polarization-duplexing-based STAR gives up the polarization domain for one-way data multiplexing, however. In addition, channel reciprocity is lost because the Tx and Rx have different polarizations, and their feed ports are placed at different locations on the antenna. This article will subsequently review recent research advances at Columbia University on integrated nonmagnetic passive CMOS circulators and antennas for STAR radios [18]–[20], [26], [27]. The integrated FD radio in [16] is also highlighted for implementing a compact active-circulator-based integrated shared-antenna interface.

Achieving >100-dB SI Suppression

Based on the maximum Tx power and the Rx sensitivity that must be supported by the application, >110-dB SI suppression can be required. Ideally, the SI suppression must be achieved without any additional power, noise,

and linearity penalty. Additionally, such a high level of SI suppression must be performed across multiple domains (such as antenna, RF, analog, and digital), as obtaining such a high level of precision using a single domain or circuit is prohibitive from a circuit complexity or power consumption perspective. The suppression must be judiciously distributed across the domains, as suppression in one domain relaxes the dynamic range requirements of the domains downstream.

Furthermore, all cancellation circuits must be adaptively configured together. Optimizing the performance of a single cancellation stage alone can result in residual SI that is suboptimal for the cancellers downstream. Research efforts that rely on commodity hardware have examined these challenges [2], [9], [11], [12] and demonstrated >100-dB SI suppression. In the context of integrated FD radios, we have examined joint cancellation across the antenna, RF/analog, and digital domains, at both RF [19], [20] and millimeter-wave (mm-wave) frequencies [18], and demonstrated 80–90-dB SI suppression levels.

SI Channel Frequency Selectivity and Wideband RF/Analog SI Cancellation

The wireless SI channel can have a response that varies substantially in magnitude and phase over the signal BW of interest. Compact antennas can be quite frequency selective, and the front-end filters necessary in today's radios to mitigate out-of-band interference are even more so. The wireless SI channel also includes environmental reflections, resulting in a delay spread that can extend to very long delays, particularly in indoor environments. Performing wideband RF/analog cancellation requires recreating the frequency response of the wireless SI channel in the RF/analog domain.

Conventional analog/RF cancellers feature a frequency-flat magnitude and phase response and will, therefore, achieve cancellation only over a narrow BW. Wideband SIC at RF based on time-domain equalization [essentially an RF finite impulse response (FIR) filter] has been reported in [2] using discrete components. However, the integration of nanosecond-scale RF delay lines on an IC is a formidable (perhaps impossible) challenge, and, therefore, alternate wideband analog/RF SIC techniques are required. In [33], we demonstrated integrated SIC in the RF domain across a wide SI BW using a frequency-domain equalization technique that channelizes the signal BW into sub-bands and then emulates the wireless SI channel in each sub-band using programmable RF bandpass filters (BPFs) based on N-path filter technology.

Transceiver Nonidealities

The extremely powerful nature of SI exacerbates the impact of nonidealities, such as nonlinearity and phase noise, particularly for IC implementations (Figure 1). For instance, nonlinearity along the Tx chain will introduce distortion products. Antenna and RF cancellation that taps from the output of the Tx will suppress these distortion products, but linear digital cancellation will not, as it operates on the undistorted digital signal. Depending on the amount of antenna and RF cancellation achieved, the analog Rx front end may introduce distortion products as well—as may the RF cancellation circuitry.

Nonlinear digital cancellation may be employed to recreate and cancel these distortion products, but the associated complexity and power consumption must be considered. Local oscillator (LO) phase noise can pose problems as well. If a common LO is used for the Tx and the Rx, the phase noise in the transmitted and the received SI will be completely correlated, enabling its cancellation in the Rx downmixer. However, delay in the SI channel will decorrelate the phase noise, resulting in residual SI that cannot be cancelled. A discussion of these challenges for integrated FD radios may be found in [14] and [15]. The integrated FD radio in [17] is noteworthy in that it emphasizes the linearity of the Rx front end and the analog SI cancellers, enabling the handling of high SI power levels. The impact of phase noise is discussed in [34] and [35].

Adaptive Cancellation

The SIC in all domains must be reconfigurable and automatically adapt to changing operation conditions (e.g., supply voltage and temperature) and, most importantly, a changing electromagnetic (EM) environment (i.e., wireless SI channel), given the high level of cancellation required. This requires the periodic (or, perhaps, even continuous) usage of pilot signals to characterize the SI channel, the implementation of reconfigurable cancellers which is more challenging in the antenna and RF domains), and the development of cancellers adaptation algorithms. Adaptive canceller tuning algorithms are described in [2] and [36], among others.

Resource Allocation and Rate Gains for Networks with Integrated FD Radios and Rethinking Medium Access Control Protocols

The benefits of enabling FD are clear: the uplink (UL) and downlink (DL) rates can theoretically be doubled (in both random-access networks, e.g., Wi-Fi, and small-cell networks). That, of course, is true, provided that the SI is cancellers such that it becomes negligible at the Rx. Hence, most research on FD at the higher layers has focused on designing protocols and assessing the capacity gains while using models of recent laboratory benchtop FD implementations (e.g., [2]) and assuming perfect SI cancellation. However, given the special characteristics of IC-based SI cancelers, there is a need to understand the capacity gains and develop resource allocation algorithms taking these characteristics into account. These

algorithms will then serve as building blocks for the redesign of medium access control (MAC) protocols for FD networks with integrated FD radios.

Overview of the Columbia FlexICoN Project

The interdisciplinary FlexICoN project was started at Columbia University in 2014 to investigate the feasibility of practical small-form-factor integrated FD radio implementations and to address the important cross-layer challenges stemming from the need to design compact ICs and to jointly design the MAC and physical layers. We have developed

1) novel antenna interfaces, such as integrated CMOS nonreciprocal circulators that utilize time-variance to break Lorentz reciprocity, and a polarization-based antenna cancellation technique that achieves wideband isolation that can be reconfigured as the environment changes
2) several generations of RF and mm-wave FD transceiver ICs that employ RF/analog self-interference cancellation circuits that combat noise, distortion, and BW limitations
3) higher layer resource allocation algorithms that evaluate FD rate gains given realistic physical layer models
4) demonstrations of FD operation using realistic IC-based nodes.

Figure 2 depicts an overview of the interdisciplinary project, highlighting some of the advances on the IC and testbed evaluation fronts.

Compact Polarization-Duplexed STAR Antennas Employing Reconfigurable SI Cancellation

SI suppression within the antenna interface is crucial in order to relax the dynamic range requirements on the RF, analog, and digital blocks in the Rx chain as well as the RF/analog and digital SIC circuits. The antenna interface should be compact and provide SI suppression over wide BWs while preserving radiation patterns. Additionally, it should maintain SI suppression in the presence of a changing EM environment.

Initial approaches to improve the isolation at the antenna interface have relied on multiple transmitting antennas that create a destructive interference at the receiving end [37]. Another approach focuses on suppressing SI right at the antenna interface using antenna isolation improvement techniques, such as [38] and [39]. Having multiple Tx antennas imposes several disadvantages, however. First, using multiple antennas for

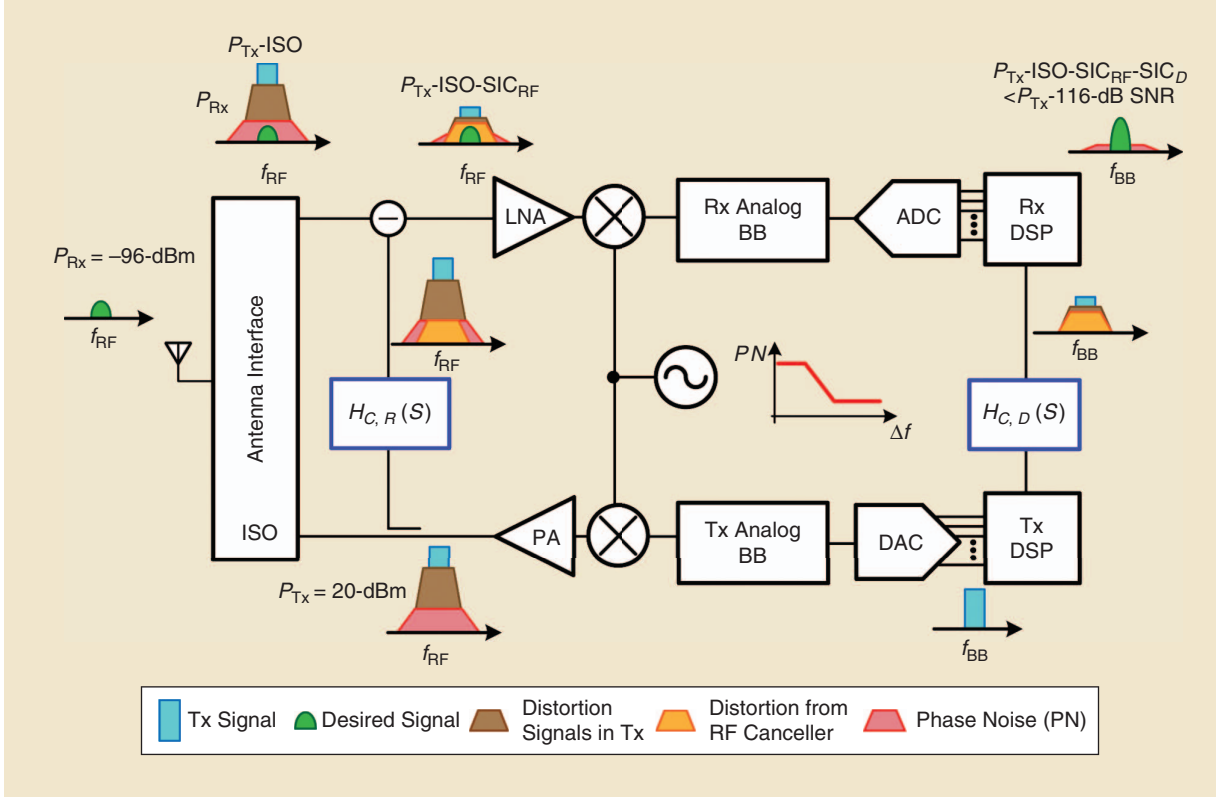

Figure 1. *An overview of the various nonidealities and challenges associated with the design of integrated FD transceivers. LNA: low-noise amplifier; PA: power amplifier; BB: baseband; SNR: signal-to-noise ratio; ADC: analog-to-digital converter; DSP: digital signal processor; DAC: digital-to-analog converter; ISO: isolation.*

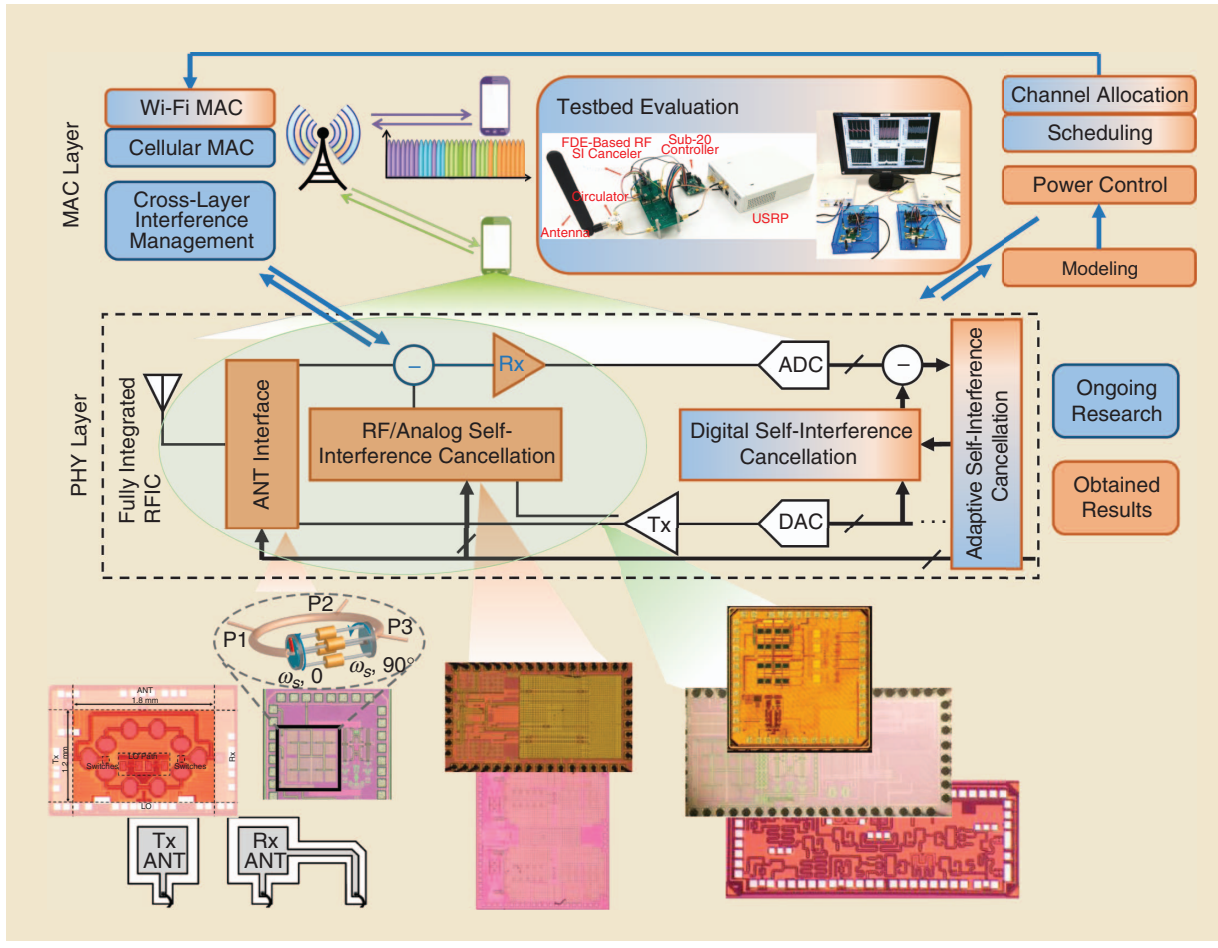

Figure 2. *An overview of Columbia's FlexICoN project. PHY: physical; ANT: antenna; USRP: universal software radio peripheral.*

the Tx requires additional active circuitry. Second, the form factor of the FD transceiver is further increased due to the extra antenna(s). Third, the Tx far field radiation pattern might be altered, as the beamforming weights are selected for destructive interference at the Rx. Finally, the isolation degrades in the presence of multipath reflections. Isolation degradation due to multipath is also seen in the case of isolation enhancement techniques, such as in [38].

Another approach that has recently gained more interest is to achieve high isolation right at the antenna using polarization-based duplexing either through stacked or multifeed antennas [14], [24], [32]. However, to get wideband isolation, especially at mm-wave frequencies, additional RF cancellation is required early in the Rx chain. Additionally, due to the lack of reconfigurability, the effect of a changing EM environment can be detrimental in these cases as well. Such polarization-based STAR approaches sacrifice the ability to use the polarization dimension to multiplex data in one dimension. Hence, while they do enable STAR functionality, we refrain from using the term *FD* to describe them.

To address all requirements of the antenna interfaces, we proposed a wideband, reconfigurable, polarization-based antenna interface for STAR. Figure 3(a) depicts the proposed technique, which employs a compact colocated Tx and Rx antenna pair with orthogonal polarizations to enhance the inherent Tx-to-Rx isolation. Additionally, an auxiliary port copolarized with the Tx antenna is introduced on the Rx coupling path between the Tx and Rx ports. The signal in the indirect path is adjusted through a reconfigurable reflective termination as it couples to the Rx port, cancelling the SI through the direct path. By employing a higher-order reflection termination, our technique can mimic the direct path magnitude and phase as well as their slopes at multiple frequency points to achieve wideband SI cancellation similar to the frequency-domain equalization (FDE) technique described previously. The electronically programmable nature of this reflective termination also allows SIC to be maintained in the presence of a changing EM environment.

A 4.6-GHz antenna prototype employing this technique was built [Figure 3(b)] and achieves greater than 50-dB isolation over a 300-MHz BW. This represents a

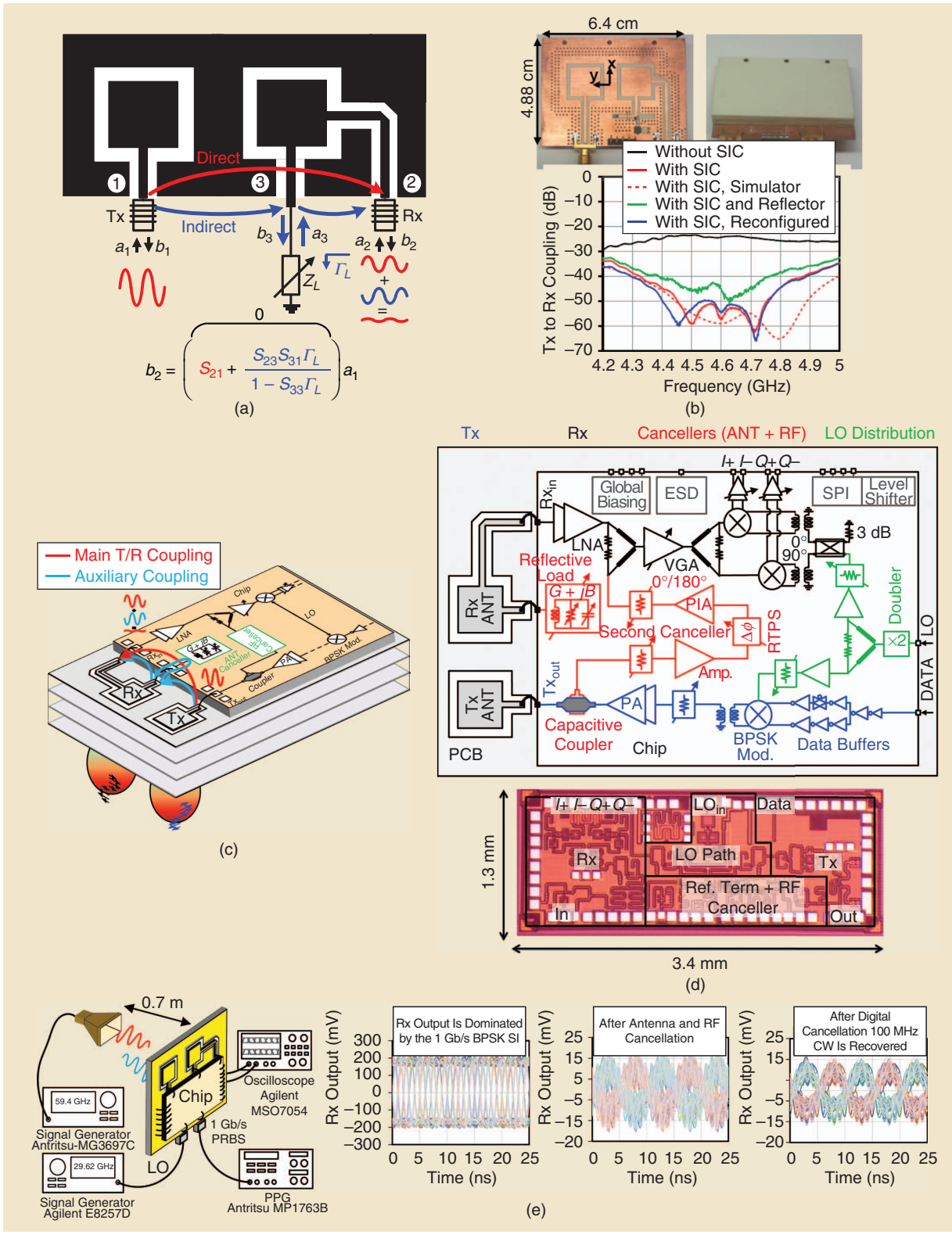

Figure 3. *Polarization-based reconfigurable wideband antenna cancellation: (a) the concept, (b) a 4.6-GHz Tx/Rx antenna pair prototype and associated measurement results, (c) a 3D implementation view of a 60-GHz FD transceiver employing the proposed antenna cancellation, (d) a 60-GHz fully integrated 45-nm SOI CMOS FD transceiver architecture and IC microphotograph, and (e) a 60-GHz FD link setup and demonstration. T/R: transmit/receive; ESD: electrostatic discharge; VGA: variable-gain amplifier; RTPS: reflection type phase-shifter; Mod.: modulator; SPI: serial peripheral interface; PIA: phase-inverting amplifier; PPG: pulse-pattern-generator; PRBS: pseudo-random binary sequence.*

20× improvement in isolation BW over conventional techniques. A 60-GHz prototype for the same technique was implemented using PCB antennas [18], demonstrating that the proposed technique can be readily scaled up in frequency. As depicted in Figure 3(c), the reconfigurable reflective termination is implemented on a 45-nm silicon-on-insulator (SOI) CMOS chip that also integrates a 60-GHz transceiver. To improve the SI suppression further, an RF canceller from the Tx output to the low-noise amplifier (LNA) output is also included in the transceiver. The complete 60-GHz FD transceiver architecture and its chip microphotograph are shown in Figure 3(d).

In conjunction with digital SIC implemented in MATLAB, a total SI suppression of nearly 80 dB was achieved over 1-GHz BW, enabling the first mm-wave FD link over a distance of almost 1 m. Figure 3(e) shows the demonstration setup using a 100-MHz offset continuous-wave (CW) signal and 1-Gb/s binary phase-shift keying (BPSK) as the desired and transmitted signal, respectively. In the absence of antenna and RF SIC, the Rx output is dominated by the transmitted signal SI. Engaging the antenna, RF and digital SIC allow reception of the desired signal with a signal-to-interference-noise-and-distortion ratio of 7.2 dB.

Enabling Shared-Antenna Full Duplex Using Integrated Nonmagnetic Circulators

As mentioned previously, early FD demonstrations used antenna pairs [40] or nonreciprocal ferrite-based circulators [2] as their respective antenna interfaces.

Reciprocal Shared-Antenna Interfaces

Shared-antenna interfaces are desirable, as they are more compact, ensure channel reciprocity, and are compatible with antenna diversity and MIMO concepts.

EBDs are transformer-based reciprocal shared-antenna interfaces that enable STAR functionality by providing isolation between the Tx and Rx through a balance impedance. However, reciprocal, matched three-port networks cannot be lossless; hence, EBDs feature a theoretical 3-dB loss in the Tx–antenna and antenna–Rx transmission paths. Practically, due to implementation nonidealities such as metal resistivity and substrate loss, the transmission losses increase by an additional 0.5–1 dB. In special cases, these losses can be made asymmetrical to favor either Tx–antenna or Rx NF performance. EBDs offer additional benefits, such as high linearity without any dc power consumption and adaptive isolation through the use of reconfigurable balance networks [14], [28]–[31].

Nonreciprocal Shared-Antenna Interfaces

Overcoming the fundamental 3-dB loss limitation requires breaking reciprocity. Conventional nonreciprocal shared-antenna FD interfaces, however, i.e., nonreciprocal ferrite-based circulators, rely on magnetic materials that are incompatible with CMOS technology and are thus bulky and expensive.

Therefore, there is a need for nonreciprocal shared-antenna FD interfaces that are CMOS-compatible and have low loss and support high Tx power levels. Furthermore, integrating the antenna interface on the same CMOS platform as the rest of the transceiver allows for a joint design and optimization of the radio as a whole and also allows for a fresh look into some long-held front-end design mantras.

Breaking Lorentz Reciprocity

Lorentz reciprocity is a fundamental characteristic of electronic structures that are linear time-invariant, passive, and based on conventional materials with symmetric permittivity and permeability tensors. Traditionally, nonreciprocity has been achieved using the magneto-optic Faraday effect in ferrite materials. A mentioned previously, however, ferrite materials are incompatible with CMOS fabrication processes. Early efforts to enable magnetic-free nonreciprocity used the inherent unilateral nature of active voltage-/current-biased transistors [41]. Active circulators are limited in their linearity and noise performance, and are therefore not suitable for radio applications with stringent linearity and noise requirements. Recently, it has been shown that violating time-invariance within a linear, passive, and nonmagnetic material, specifically by spatiotemporal modulation of material permittivity, can introduce nonreciprocal wave propagation and enable the construction of circulators [42]–[44]. Electronic circuit realizations of this concept at RF employ varactors for permittivity or capacitance modulation. Permittivity modulation is inherently very weak, however, resulting in a tradeoff between loss and tuning range in CMOS varactors. Consequently, these efforts have resulted in designs that exhibit a tradeoff between loss, linearity, size, and BW.

Recently, we introduced a new approach to nonmagnetic CMOS-compatible nonreciprocity based on spatiotemporal conductivity modulation using passive transistor-based switches [19], [20], [26], [27], [45]. Conductivity in semiconductors can be modulated over a wide range (the CMOS switch resistance ON/OFF ratio can be as high as $10^{-3} - 10^{-5}$) relative to permittivity [42] (varactor C_{max}/C_{min} is typically 2–4). In the rest of this section, we will cover our recent research on linear, periodically time-varying (LPTV) switch-based high-performance passive nonmagnetic circulators over RF to mm-wave frequencies in CMOS. We will describe the fundamental physical principles as well as three generations of CMOS circulators and circulator-based wireless systems targeting emerging FD and 5G mm-wave applications.

Nonreciprocity Based on Staggered Commutation

N-path filters have recently reemerged as a promising solution to enable the implementation of tunable, high-quality-factor filters at RF in nanoscale CMOS IC technology [46]. N-path filters are a class of LPTV networks in which the signal is periodically commutated using passive transistor switches through a bank of capacitors. As that occurs, a second-order BPF profile is created through the translation of the low-pass filtering of the capacitor to a center frequency defined by the clock frequency. We have found that applying a relative phase shift to the nonoverlapping clocks driving the input and output switch sets of a two-port N-path filter imparts a nonreciprocal phase shift to the signals traveling in the forward and reverse directions because they see a different ordering of the phase-shifted switches (lead-lag versus lag-lead). The magnitude response remains reciprocal, and there is low-loss tunable filtering, similar to traditional N-path filters [Figure 4(a)].

To convert phase nonreciprocity into nonreciprocal wave propagation, an N-path-filter with $\pm 90^\circ$ phase-shift is placed inside a transmission-line loop with a length of $3\lambda/4$ [Figure 4(b)]. The combination of the nonreciprocal phase shift of the N-path filter with the reciprocal phase shift of the transmission line results in supporting unidirectional wave propagation ($-270^\circ - 90^\circ = -360^\circ$), because the boundary condition for wave propagation in the reverse direction cannot be satisfied ($-270^\circ + 90^\circ = -180^\circ$). Additionally, a three-port circulator can be realized by placing ports anywhere along the loop, as long as they maintain a $\lambda/4$ circumferential distance between them, resulting in the following S-parameters at the center frequency of operation (f_s):

$$S_{\text{circ}}(f_s) = \begin{bmatrix} 0 & 0 & -1 \\ -j & 0 & 0 \\ 0 & -j & 0 \end{bmatrix}. \tag{1}$$

Additionally, for a given Tx excitation $V_{\text{in,tx}}$, the voltages on either side of the N-path filter (V_x, V_y) have a magnitude of $(\sin(\beta l)\, V_{\text{in,tx}}/2)$, where β and l are the propagation constant of the $3\lambda/4$ ring and the distance from the Rx port to the N-path filter, respectively [Figure 4(b)]. This result suggests that, by setting l to zero (placing the Rx port adjacent to the N-path filter), the inherent Tx-to-Rx isolation suppresses the voltage swing on either side of the N-path filter, enhancing its linearity with respect to the Tx port.

A prototype circulator operating over 610–850 MHz was implemented in a 65-nm CMOS process [Figure 4(c)–(d)]. The N-path filter was implemented using eight paths. Each $\lambda/4$ transmission line was replaced with a lumped capacitor-inductor-capacitor (CLC) section, in which the inductors were placed off chip to achieve a better quality factor. The measurements shown in Figure 4(e) reveal 1.7 dB loss in Tx–antenna and antenna–Rx transmission and broadband isolation better than 15 dB between the Tx and Rx (the narrowband isolation can be as high as 50 dB using an antenna tuner). The in-band antenna–Rx third-order input intercept point (IIP3) is +8.7 dBm while the in-band Tx–antenna IIP3 is +27.5 dBm, nearly two orders of magnitude higher due to the voltage swing suppression across the N-path filter [Figure 4(f)]. The measured clock feedthrough to the antenna port is –57 dBm and in-phase/quadrature (IQ) image rejection for Tx–antenna transmission is 49 dB.

Topics for future research include enhancing BW and Tx power handling, improving the rejection of spurs, and incorporating antenna tuning functionality into the circulator. A new architecture with enhanced BW is discussed in the "Wideband mm-Wave Nonreciprocity Based on Generalized Spatio-temporal Conductance Modulation" section. Using SOI CMOS technologies in conjunction with switch-linearization approaches can further enhance the Tx–antenna linearity and power handling. Using these techniques, we have demonstrated a circulator with high Tx–antenna linearity (IIP3 > 50 dBm) and reconfigurable isolation across 1.85 voltage standing wave ratio at 1 GHz in [47]. Clock feedthrough and IQ mismatch can be calibrated by sensing and injecting appropriate baseband (BB) signals through the N-path filter capacitor nodes, as shown previously in the literature [48].

Rx With Integrated Magnetic-Free Circulator and BB Self-Interference Cancellation for FD Wireless

A 610–850-MHz FD Rx IC prototype incorporating the nonmagnetic N-path, filter-based passive circulator described previously and additional analog BB SI cancellation [shown in Figure 5(a) and (b)] was also designed and fabricated in the 65-nm CMOS process [19]. Through a joint optimization over a BW of 12 MHz, 42 dB of SI suppression is achieved across the circulator and analog BB SIC. The NF of the overall FD Rx is 10.9 dB while consuming 160 mW of dc power.

Digital SIC has also been implemented in MATLAB after capturing the BB signals using an oscilloscope (an 8-b quantizer) for a two-tone Tx signal [Figure 5(c)]. The digital SIC cancels not only the main SI but also the 3rd order intermodulation (IM3) distortion generated on the SI by the circulator, Rx, and canceller. A total of 164 canceller coefficients are trained and calculated. After digital SIC, the main SI tones are at the –92-dBm noise floor, while the SI IM3 tones are 8 dB below, for –7-dBm Tx average power. This corresponds to an overall SI suppression of 85 dB for the FD Rx.

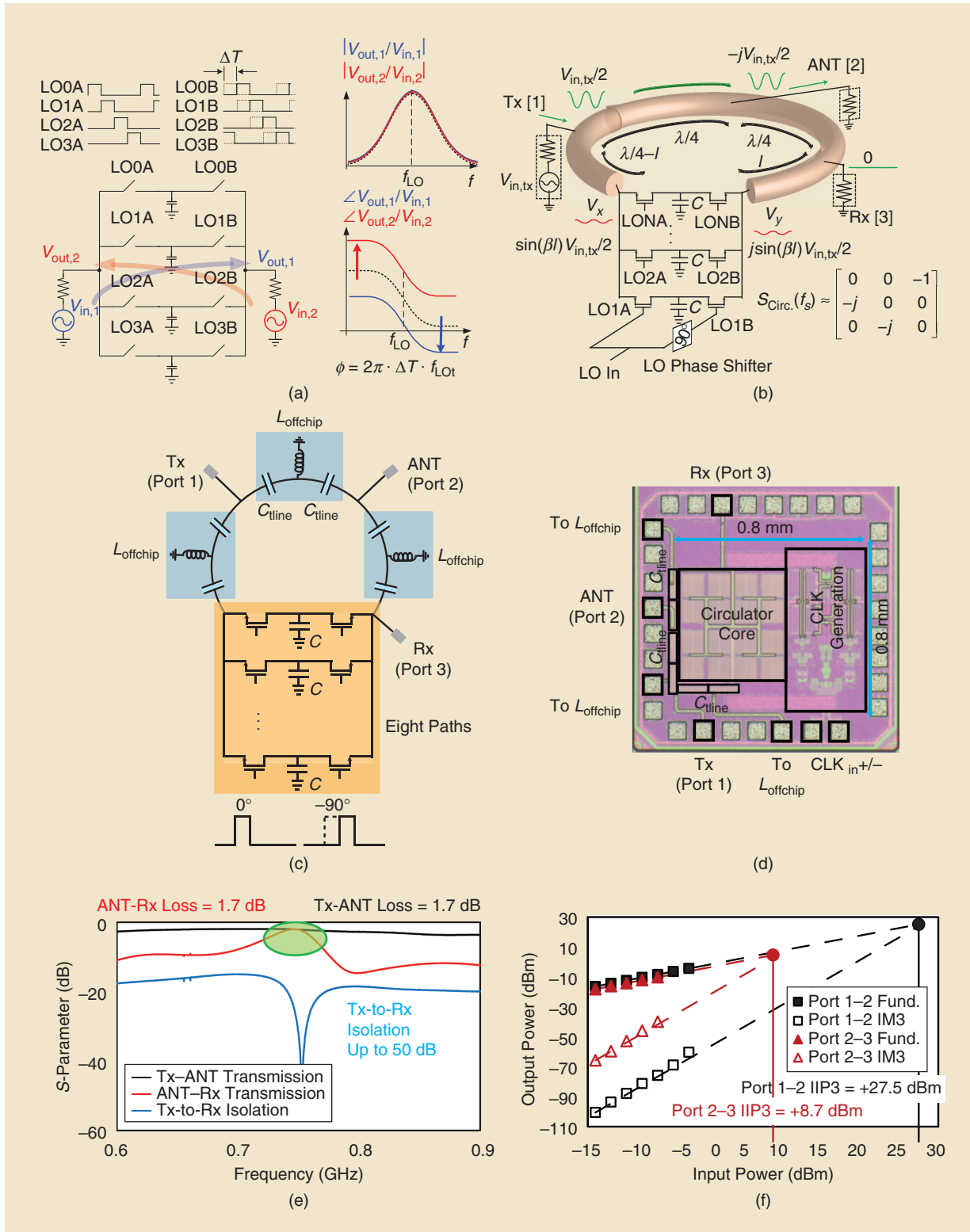

Figure 4. *An integrated nonmagnetic N-path, filter-based circulator for single-antenna FD: (a) the nonreciprocity induced by phase-shifted N-path commutation; (b) a 3-port circulator structure obtained by placing the nonreciprocal two-port N-path filter with ±90° phase shift within a 3λ/4 transmission line loop; (c) the miniaturization of the 3-port circulator by replacing each λ/4 transmission line with a lumped CLC section; (d) a chip microphotograph of the 65-nm CMOS 610–850-MHz circulator (inductors placed off chip); (e) the circulator S-parameter measurements; and (f) a comparison of Tx–antenna and antenna–Rx IIP3 measurement results. CLK: clock; Fund.: fundamental.*

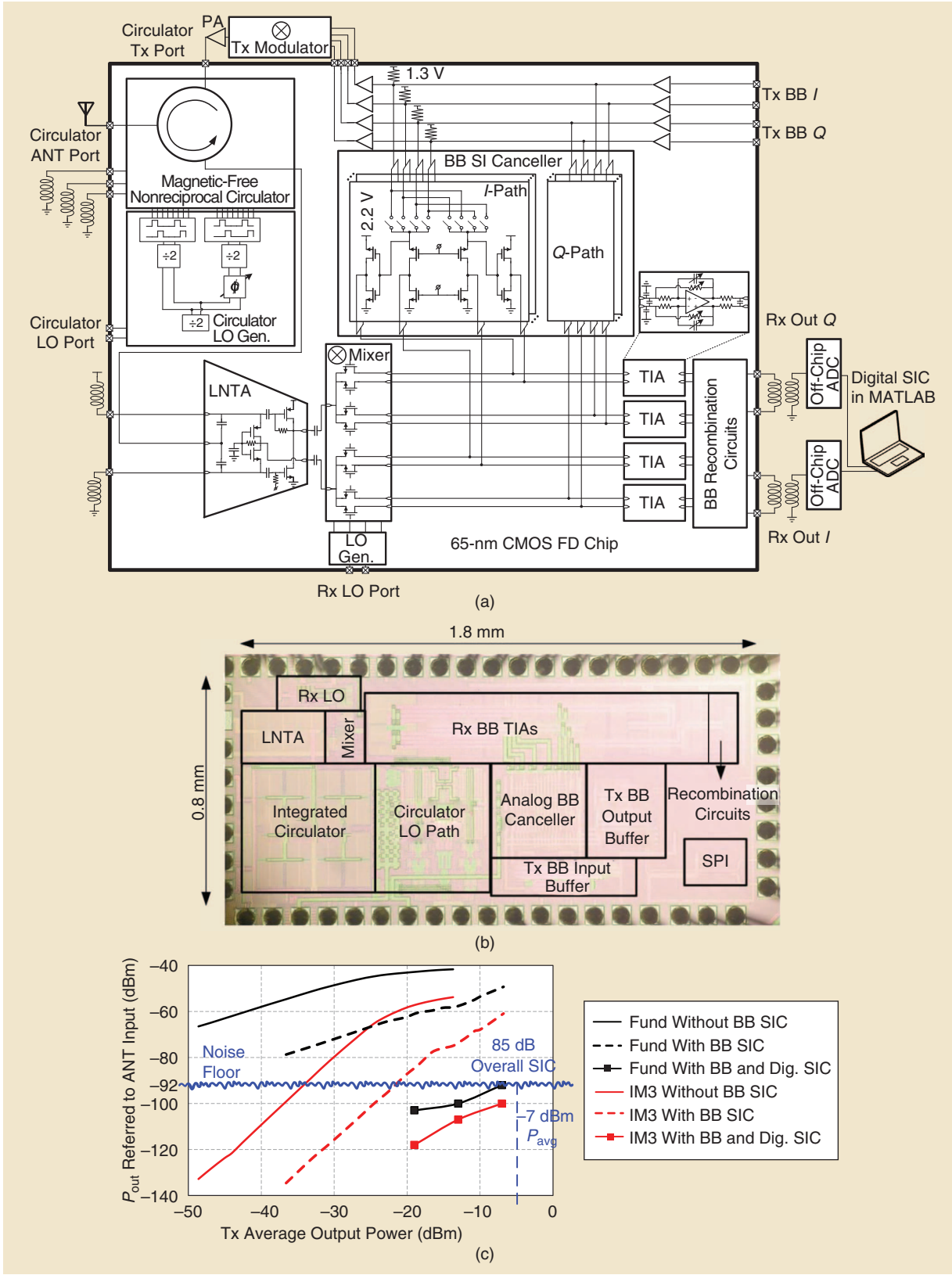

Figure 5. *(a) A block diagram and schematic of the implemented 65-nm CMOS 610–850-MHz FD Rx with nonmagnetic circulator and additional analog BB SI cancellation; (b) the chip microphotograph; and (c) the measured two-tone SI test, with SI suppression across the circulator, analog BB, and digital domains. TIA: transimpedance amplifier; Gen.: generator; LNTA: low noise transconductance amplifier; Dig.: digital.*

Integrated Magnetic-Free Circulator-Rx

As mentioned previously, integration of the circulator on the same chip as the FD radio opens new pathways to codesign and cooptimize the overall front end. In [20], we have reported a new FD architecture that we call a *circulator-Rx*. Our design benefits from merging the antenna interface, downconverter, and antenna impedance tuner into a single block.

Reciprocal antenna interfaces, such as surface acoustic wave duplexers and filters, mandate 50-Ω matching at the Tx and Rx ports to obtain the best filtering performance and provide antenna matching. A nonreciprocal circulator breaks this traditional 50-Ω matching requirement at the Rx, however, because the unabsorbed Rx power circulates away from the antenna. This can substantially simplify LNA design and improve noise performance, as simultaneous noise and impedance matching is a substantial challenge in LNA design.

Another interesting feature of our circulator is the inherent downconversion functionality embedded into its structure. The N-path filter not only provides nonreciprocal phase shift but also can be repurposed as the downconverting mixer, directly providing the BB signals on its capacitors [Figure 6(a)]. The structure becomes equivalent to a circulator merged with a zero-intermediate frequency, mixer-first Rx, offering the additional advantage of not having to achieve 50-Ω input matching in the Rx [Figure 6(b)]. An additional interesting behavior is noise circulation, also shown in Figure 6(b). It can be proven that the noise of the Rx-side switches alone contribute to Rx NF, while the noise of the Tx-side switches circulates away. Hence, the NF of the circulator-Rx is theoretically as low as

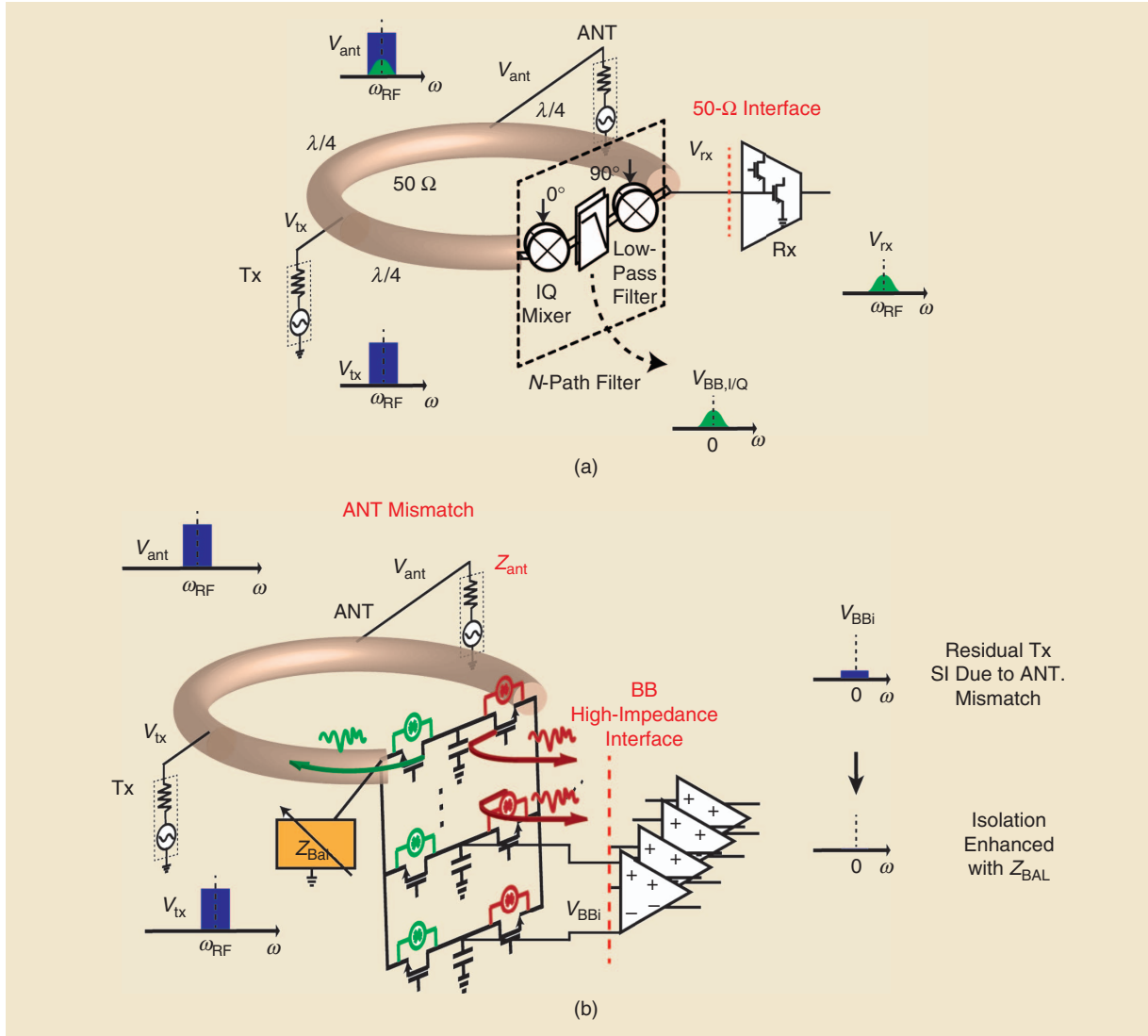

Figure 6. *(a) The circulator-Rx concept: the downconverted signal exists within the circulator structure on the BB capacitors of the N-path filter. (b) Some innovations of the circulator-Rx: embedded antenna balancing and the noise circulation concept.*

that of traditional mixer-first Rxs despite the additional set of switches. Finally, it should be mentioned that the Tx maintains isolation to the BB nodes in this structure and the Tx–antenna linearity enhancement will still be observed. These innovations result in a lower power consumption and NF for the FD Rx due to the elimination of the traditional LNA/mixer and their associated noise sources.

In the face of antenna variations, all circulators require an antenna tuner to maintain Tx-to-Rx

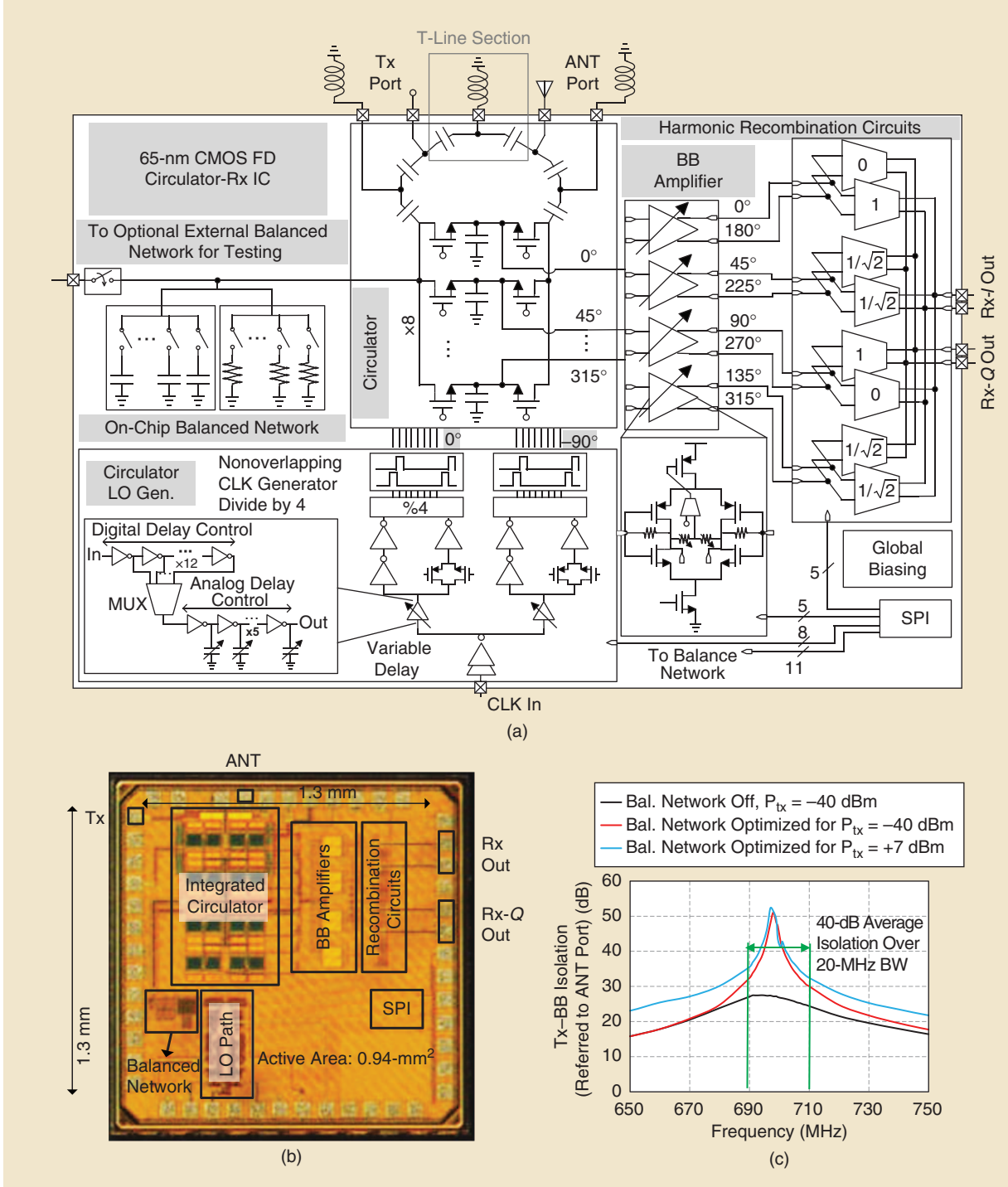

Figure 7. *(a) A block diagram and schematic of the implemented 65-nm CMOS 610–975-MHz FD circulator-Rx, (b) the chip microphotograph, and (c) the measured Tx-to-Rx BB isolation referred to the antenna port with and without the balance network and for various Tx power levels. Bal.: balance; Ptx: power transmitter; MUX: multiplexer; SPI: serial peripheral interface.*

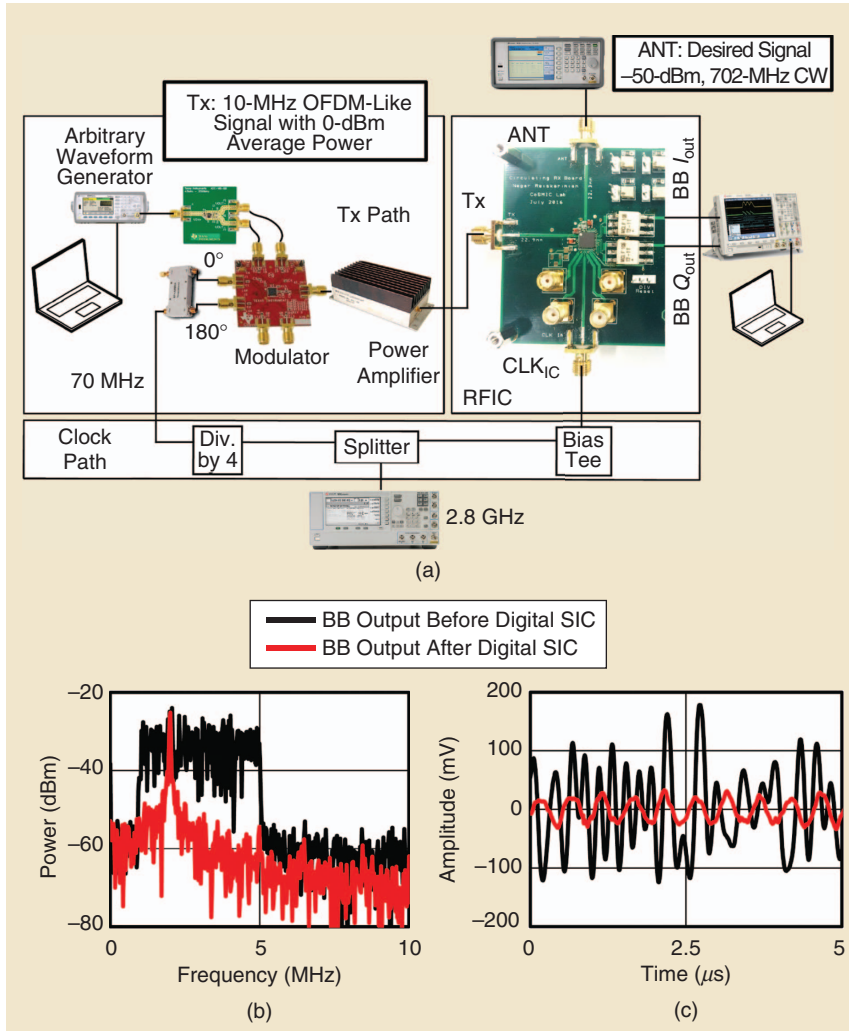

Figure 8. *(a) An FD demonstration using the circulator-Rx IC. (b) and (c) demonstrate that a –50-dBm weak desired signal is received while transmitting a 0-dBm average-power OFDM-like signal.*

isolation. Inspired by the concept of the balanced network in EBDs [31], we have found that incorporating a tunable impedance on the Tx side of the N-path filter can maintain Tx-to-Rx isolation as the antenna impedance varies [Figure 6(b)]. The balanced network is engineered to create a reflection path, which cancels out the Tx–BB leakage. Engaging the balanced network results in higher linearity as higher suppression of the Tx SI is achieved prior to the first BB amplifier, particularly in the presence of antenna mismatch.

A 610–975-MHz prototype circulator-Rx was designed and fabricated in 65-nm CMOS technology, as shown in Figure 7(a) and (b). The N-path filter BB nodes are amplified by inverter-based BB amplifiers and harmonic recombination circuitry. The on-chip balance network consists of a tunable resistive and capacitive bank. Measurements of the Tx–antenna path reveal 1.8-dB loss and +30-dBm IIP3. The average small-signal Tx–BB isolation (referred to the *antenna port*) is, at best, approximately 25 dB, as shown in Figure 7(c). Engaging and optimizing the balance network dramatically improve the average small- and large-signal isolation to 40 dB over a 20-MHz BW. A more comprehensive balanced network with wider impedance variation and inductive elements, such as those investigated previously for EBD [31], can enable coverage of wider antenna impedance variation. The overall NF of the circulator-Rx is 8 dB, the power consumption is 108 mW (reduced by approximately 35% compared to our prior work), and the Tx power handling is +8 dBm (improved 30 × compared to our prior work).

We have also shown an FD demonstration using our RFIC and a commercial, off-the-shelf component-based Tx, as shown in Figure 8(a). A 0-dBm average-power orthogonal frequency-division multiplexing (OFDM)-like Tx signal with five subcarriers and a 10-MHz RF BW and –50-dBm CW desired signal were concurrently fed to the Tx and antenna ports of the RFIC. The on-chip circulator provided approximately 30 dB of isolation between the Tx and Rx ports by taking advantage of the integrated balanced network. After capturing the BB signal using an oscilloscope (a 12-b quantizer), we further implemented digital SIC to show the feasibility of cancelling modulated Tx signals and recovering the desired antenna signal. To enable approximately 40-dB average SIC within the main signal BW, 315 canceller coefficients were trained. Figure 8(b) and (c) shows the frequency- and time-domain waveforms of the BB signal before and after digital cancellation. Overall, a total of 70-dB SIC was imparted to the Tx signal in the antenna interface and digital domains.

Wideband mm-Wave Nonreciprocity Based on Generalized Spatiotemporal Conductance Modulation

The mm-wave, low-loss shared antenna interfaces with FD capability as well as high linearity, isolation, and BW are extremely important in enabling small-form-factor shared Tx–Rx antenna arrays, especially for

mm-wave 5G base stations that need to communicate with multiple users simultaneously and for frequency-modulated continuous-wave automotive radars.

Inspired by the N-path filter-based low-RF CMOS circulator discussed in the previous sections, we recently proposed a near-28-GHz, fully integrated passive circulator in 45-nm SOI CMOS based on a generalized spatiotemporal conductivity modulation concept [27], [45]. Similar to the N-path, filter-based staggered commutation, this concept enables phase nonreciprocity—but uses a modulation frequency that can be substantially lower than the operation frequency (one third in this case), thus enabling mm-wave operation—and substantially enhances BW.

Figure 9 depicts the spatiotemporal conductivity modulation concept. It consists of two sets of differential mixer-quad switches on either end of a differential transmission-line delay. The switches are clocked at a modulation frequency ω_m, and the delay of the line is equal to one quarter of the modulation period ($T_m/4$). The switches are clocked with 50% duty-cycle square-wave clocks, and the clocks on the right are delayed with respect to the clocks on the left by $T_m/4$ as well. As a result, waves traveling from left to right experience the transmission-line delay with no sign flips in the first half of the clock period and two sign flips that negate each other in the second half of the clock period [Figure 9(a)]. On the other hand, waves traveling from right to left experience the transmission-line delay along with one sign flip in both halves of the clock period [Figure 9(b)]. In other words, transmission in both directions is perfectly lossless, but there is an infinitely broadband 180° nonreciprocal phase difference [Figure 9(c)].

Two key features must be highlighted:

1) The infinitely broadband phase nonreciprocity implies a broader BW of operation for the resultant

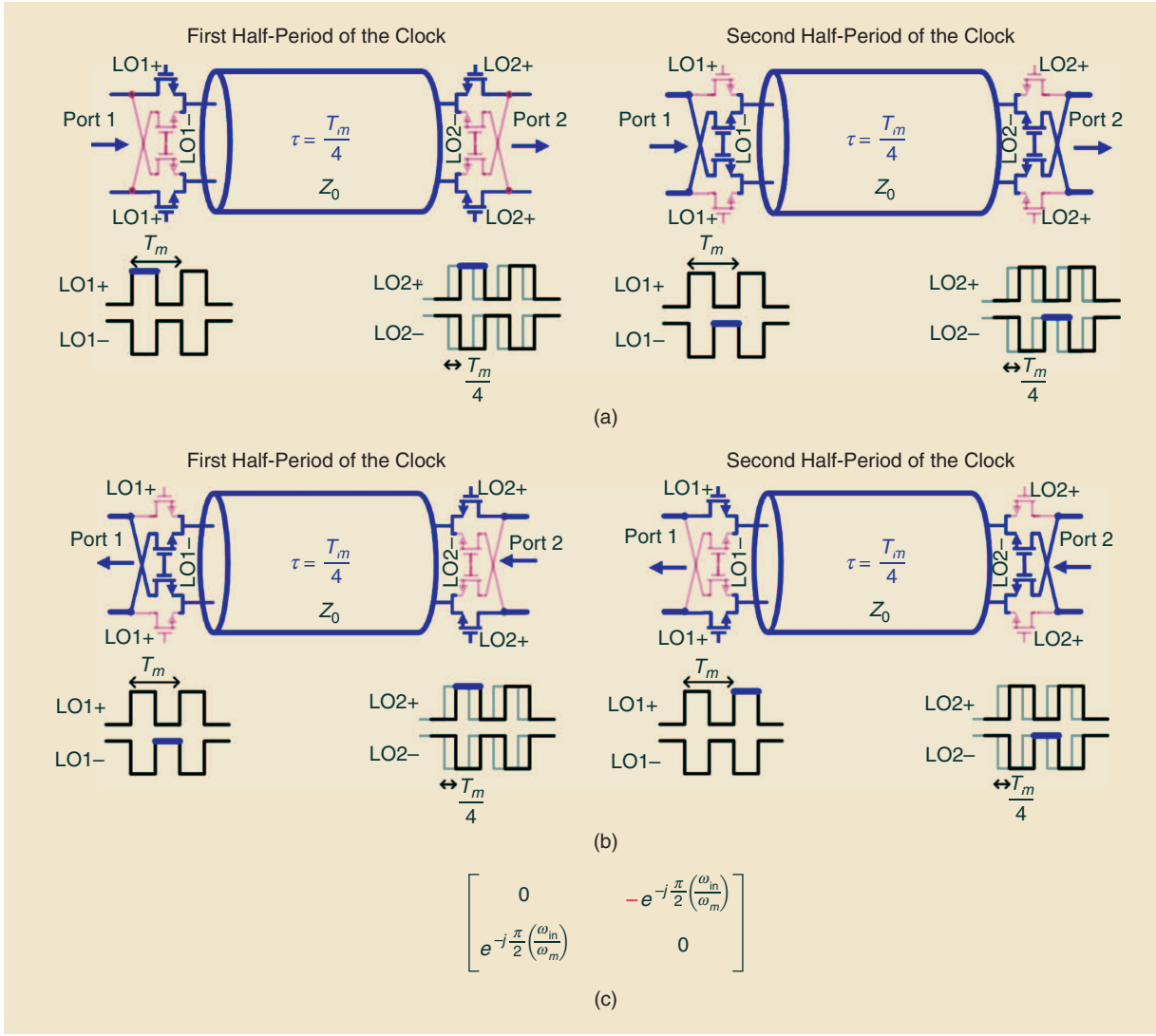

Figure 9. *The generalized spatiotemporal conductance modulation concept enables infinite BB phase nonreciprocity. (a) Propagation in the forward direction, (b) propagation in the reverse direction, and (c) the S parameters.*

circulator and the ability to modulate the switches at a frequency substantially lower than the operating frequency, allowing operation at mm-wave.
2) It is necessary to have 50% duty-cycle clocks, as opposed to numerous low-duty-cycle clocks as in N-path filters, further easing mm-wave operation.

This nonreciprocal phase shift element can now be embedded within a $3\lambda/4$ transmission-line ring to realize a nonreciprocal circulator similar to the N-path, filter-based RF circulator. For this, the nonreciprocal phase shift must be $\pm 90^{\circ}$, which requires ω_m to be an odd subharmonic of ω_{in}. Figure 10(a) shows the circulator implementation in 45-nm SOI CMOS at 25 GHz with modulation at 8.33 GHz. The differential implementation additionally reduces the LO feedthrough and improves power handling. The transmission lines are miniaturized using four stages of CLC sections. The nonreciprocal phase component is placed symmetrically between the Tx and Rx ports so that switch parasitics can be absorbed into the lumped capacitance of the $\lambda/8$ sections on either side. A two-stage polyphase filter and self-biased differential inverter chains are used to generate the 8.33-GHz square clocks.

Figure 10(b) shows the measured small- and large-signal performance of the circulator. The 25-GHz circulator achieves 3.3-/3.2-dB Tx–antenna/antenna–Rx insertion losses (ILs), respectively, and 18.3–21.2-dB of Tx-to-Rx ISO over the 4.6-GHz, 1-dB IL BW. This near-20-dB isolation is limited by reflections at the antenna port due to an imperfect termination in the measurement setup rather than the inherent isolation of the circulator itself, a challenge for all circulators. The measured antenna–Rx NF and Tx–antenna/antenna–Rx input port 1 are 3.3–4.2 dB and >21 dBm [Figure 10(b)], respectively.

Benchmarking

Comparing the performance of reciprocal and nonreciprocal antenna interfaces is not trivial since many different factors should be considered, such as loss, power consumption, NF, and linearity. To this end, we recently introduced a new metric called the *antenna interface efficiency figure of merit* [50].

Full-Duplex Testbed and Performance Evaluation

To experimentally evaluate the impact of our IC-based FD hardware research on higher layers of the network stack, we implemented two generations of the RF SI canceller using discrete components: the conventional frequency-flat RF SI canceller (Gen-1 [50]) and the FDE-based RF SI canceller (Gen-2 [51]). The discrete-component-based RF SI canceller emulate their integrated counterparts. In this section, we describe our Gen-1 and Gen-2 FD transceiver prototypes; the SI suppression across the antenna, RF, and digital domains; and a cross-layered (software and hardware) FD wireless link demonstration.

Setup

Figure 11(a) shows the diagram of an FD transceiver prototype consisting of an antenna, a ferrite circulator, a custom-designed discrete-component-based RF SI canceller, and a National Instruments (NI) USRP-2932.

The NI USRP is configured to operate at 900 MHz, which is the same as the operating frequency of both the circulator and the RF SI cancellers. The USRP is controlled from a PC that runs NI LabVIEW, which performs digital signal processing and provides a graphical user interface. Figure 11(f) and (g) shows our two generations of FD transceiver prototype [50], [51].

RF SIC

Figure 11(b) and (c) shows the diagrams of the conventional frequency-flat RF SI canceller and the FDE-based wideband RF SI canceller, both of which tap a reference signal at the output of the PA and perform SIC at the input of the LNA at the Rx side.

For the frequency-flat amplitude- and phase-based RF SI canceller, the tapped Tx reference signal is only adjusted in amplitude and phase using a variable attenuator and a phase shifter. Therefore, it can emulate the antenna interface isolation at only a single frequency point, resulting in a narrowband SIC. To achieve a wideband and more powerful RF SIC, we apply the FDE of the SI channel in the RF domain. The FDE-based RF SI canceller uses programmable BPFs to channelize the desired signal BW, as discussed previously. Within each channel, the reconfigurable BPF, along with a variable attenuator and a phase shifter, mimics the magnitude, phase, slope of magnitude, and slope of phase (i.e., group delay) of the wireless SI channel.

Figure 11(d) and (e), respectively, presents the frequency-flat RF SI canceler and FDE-based RF SI canceller implemented using discrete components. The parameters of both canceller are digitally programmable by a SUB-20 controller through the USB interface. In both implementations, the attenuator provides an attenuation range from 0 to 15.5 dB with a 0.5-dB resolution, and the passive phase shifter covers full 360° range with a 1.5° resolution.

Additionally, in the FDE-based canceller, each RF BPF uses a surface-mount coil inductor and a surface-mount thin-film capacitor that resonate at around 900 MHz with impedance transformation networks at the BPF input and output ports for a high quality factor. The center frequency and quality factor of the RF BPF are made programmable by inserting varactors in the LC resonator and impedance transformation networks, respectively.

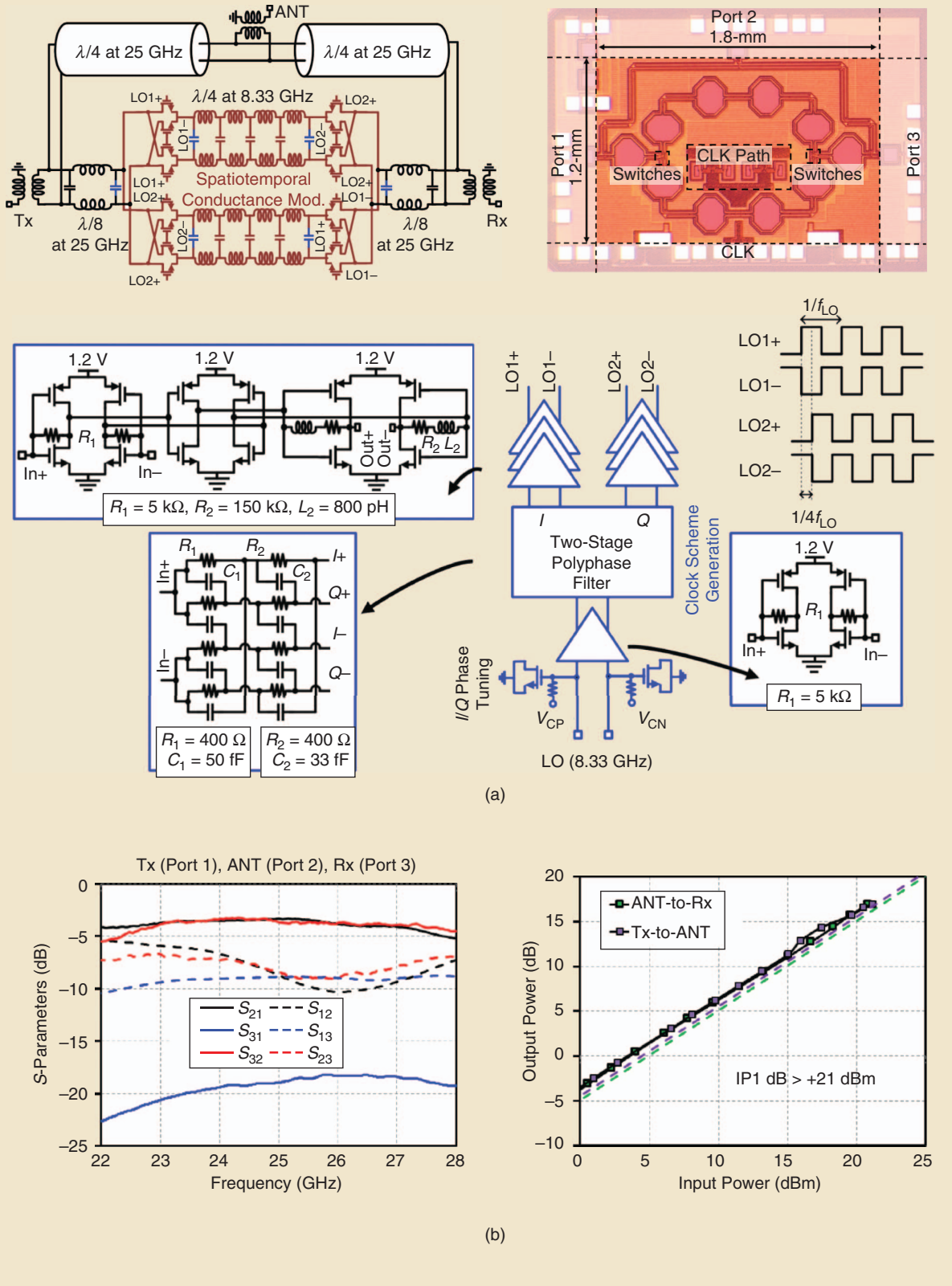

Figure 10. *(a) The block and circuit diagram and chip photo of the near-28-GHz, 45-nm SOI CMOS circulator, and (b) the measured small- and large-signal performance.*

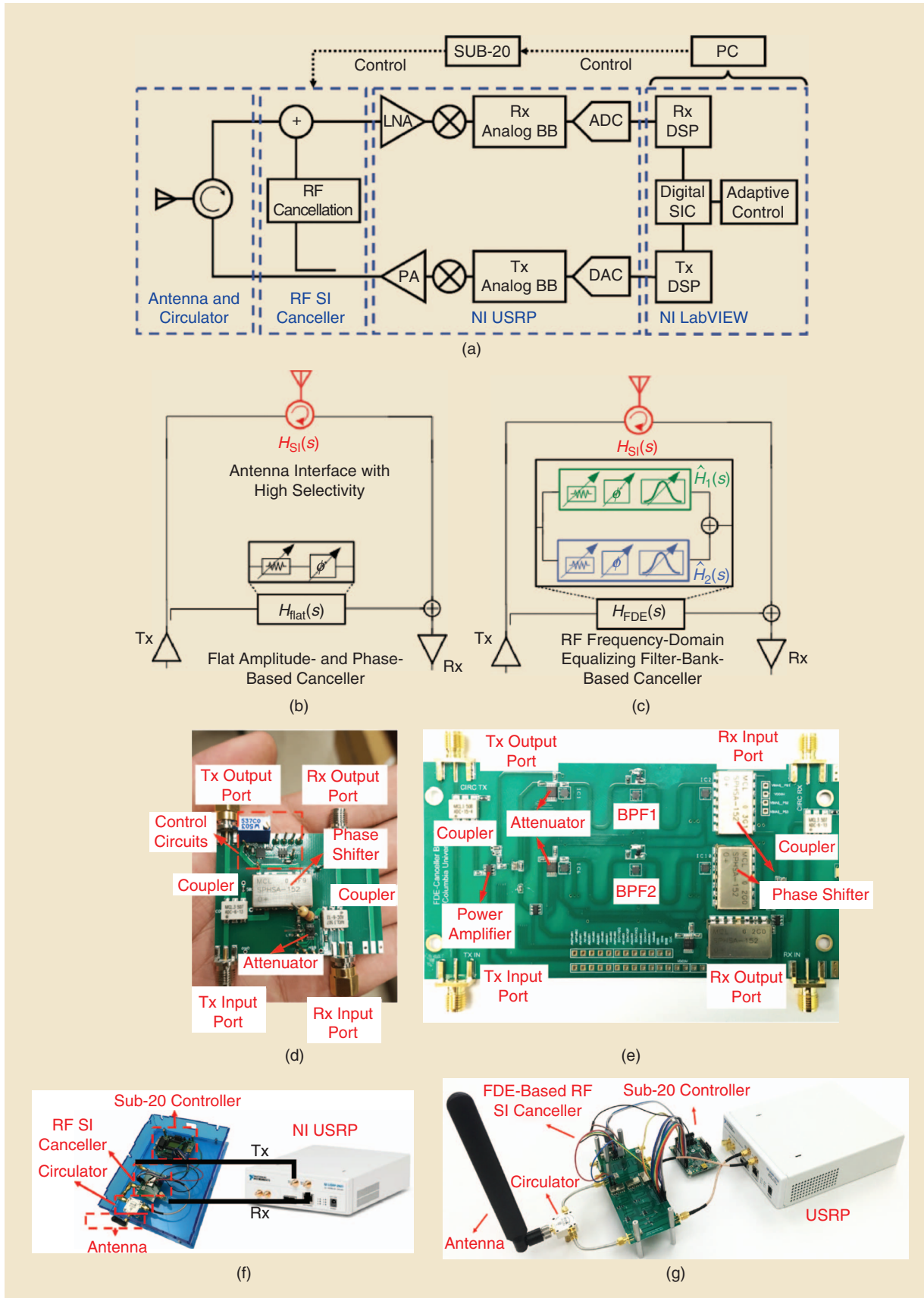

Figure 11. *(continued)*

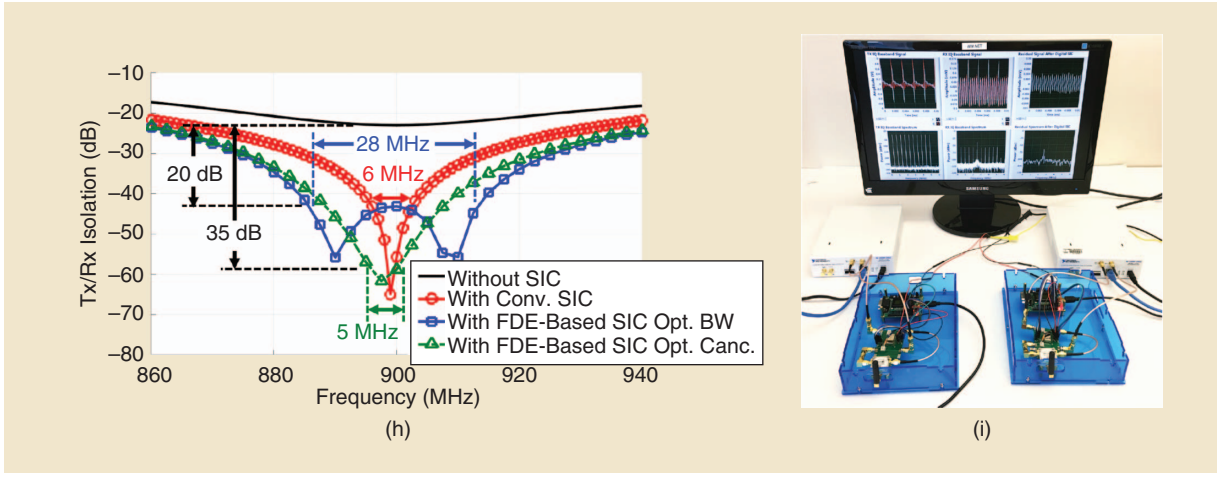

Figure 11. *(a) The block diagram of the FD transceiver prototype. (b) The block diagram of the frequency-flat, amplitude- and phase-based RF SI canceller [50]. (c) The block diagram of the FDE-based wideband RF SI canceller [51]. (d) The frequency-flat, amplitude- and phase-based RF SI canceler implemented using discrete components [50]. (e) The FDE-based RF SI canceller implemented using discrete components [51]. (f) The Gen-1 FD transceiver prototype [50]. (g) The Gen-2 FD transceiver prototype [51]. (h) The measured Tx-to-Rx isolation magnitude responses using the frequency-flat and FDE-based RF SI canceller implemented with discrete components. (i) An FD wireless link presented in [50]. Conv.: conventional; Opt.: optimum; Canc.: canceller.*

Figure 11(h) depicts the measured resulting SIC of the implemented frequency-flat and FDE-based cancellers. The measurements are performed inside an anechoic chamber to provide a stable environment so that both cancellers can achieve their best performance. Note that the FDE-based RF SI canceller can be configured to achieve wideband RF SIC (the curve labeled "Opt. BW") or to achieve higher RF SIC in a smaller BW (the curve labeled "Opt. Canc."). Figure 11(h) shows that the FDE-based canceler achieves more powerful RF SIC compared to the conventional frequency-flat canceller: it provides a 20-dB SIC BW of 28 MHz (with optimal BW), which is a 4.67× improvement over the frequency-flat canceller, or a 35-dB SIC BW of 5 MHz (with optimal cancellation).

Digital SIC

The residual SI after isolation and cancellation in the antenna and RF domains is further suppressed in the digital domain. The digital SI canceller is modeled as a truncated Volterra series and implemented based on a nonlinear tapped delay line to cancel both the main SI and the intermodulation distortion generated on the SI. Specifically, the output of the discrete-time SI canceller, y_n, can be written as a function of the current and past Tx digital BB signals, x_n and x_{n-k} (k represents the delay index), i.e.,

$$y_n = \sum_{k=0}^{N} h_{1,k} x_{n-k} + \sum_{k=0}^{N} h_{2,k} x_{n-k}^2 + \sum_{k=0}^{N} h_{3,k} x_{n-k}^3 \ldots, \quad (2)$$

where N corresponds to the maximum delay in the SI channel and $h_{i,k}\,(i = 1, 2, 3\ldots)$ is the ith order digital canceller coefficient. Using a pilot data sequence, the digital SI canceller coefficients can be found by solving the least-squares problem. The digital SIC algorithm is implemented in NI LabVIEW.

FD Wireless Link Demonstrations

In [50], an FD wireless link consisting of two Gen-1 FD transceivers was presented. We demonstrated that, for a 5-MHz (the NI USRP-2932 cannot support a higher BW when the digital signal processing is running on the host PC) multitone signal with 0-dBm average Tx power level, the SI signal was canceled to the –90-dBm noise floor by applying both the RF SIC and the digital SIC algorithm described previously. We also developed and implemented an adaptive tuning algorithm so that the frequency-flat Conv.: conventional; Opt.: optimum; Canc.: canceller adjusts to environmental changes. Figure 11(f) shows the Gen-1 FD wireless link testbed, where a total of 90-dB SI suppression was achieved. In particular, the circulator and frequency-flat RF SI canceller together provided 40-dB SI suppression before the USRP Rx, of which around 20 dB were obtained from the RF SI canceller. The additional 50-dB suppression came from the digital SIC, which eventually allowed us to detect the desired signal under the powerful SI. More recently, we have added one of our Gen-1 canceller to the ORBIT wireless testbed to enable open-access FD experimentation [53].

In [52], we presented an FD wireless link consisting of two Gen-2 FD transceivers and demonstrated 95-dB overall SI suppression in practice, enabling an FD link budget of +5-dBm average Tx power level. Specifically,

50 dB were obtained by the circulator and the FDE-based RF SI canceller across a 5-MHz BW, and 45 dB were obtained by the digital SIC. Compared with the implementation in [50], we achieved 1) higher SIC in the RF domain by using a compact FDE-based RF SI canceller and 2) 5-dB higher overall SIC supporting a 5-dB higher average Tx power level. Our ongoing work in this area is reported in [53], and future work will focus on integrating our actual IC designs into the testbed and on leveraging its flexibility for evaluation of MAC protocols.

Conclusions

Integrated FD is suitable for many applications ranging from backhaul, relays, and Wi-Fi to small-cell LTE (where cancellation requirements are relaxed compared to macro cells). The Columbia FlexICoN project has been focusing on IC-based FD transceivers spanning RF to mm-wave, reconfigurable antenna cancellation, nonmagnetic CMOS circulators, and MAC-layer algorithms based on realistic hardware models. While exciting progress has been made in the last few years by the research community, several problems remain to be solved before FD wireless can become a widely deployed reality.

Continued improvements in IC-based FD transceivers toward increased total cancellation over wide BWs and support for higher Tx power levels through improved Rx and circulator linearity are necessary. Incorporation of FD in large-scale phased-array transceivers is another open research problem, with initial progress along these lines reported in [54]. The extension of IC-based SIC concepts to MIMO transceivers is an important and formidable challenge. In a MIMO transceiver, SI will exist between every Tx–Rx pair, and a brute-force implementation will cause canceler complexity to scale quadratically with the number of MIMO elements. Our most recent work focuses on addressing this issue by exploiting area- and power-efficient passive RF and baseband active wideband MIMO cancellation with shared delay elements [55]. At the higher layers, while extensive recent research has been devoted to this area, the implications of different possible physical-layer implementations are still not fully understood. Moreover, there are still several important open problems related to MAC-layer design for both cellular and random-access networks. Specifically, it is necessary to design algorithms that support asymmetric uplink and downlink traffic requirements. In addition, it is important to consider interference management in OFDM networks jointly at the physical and MAC layers.

Acknowledgments

This work was supported in part by the DARPA RF-FPGA program, the DARPA ACT program; the DARPA SPAR program; NSF grants ECCS-1547406, CNS-1650685, and CNS-1827923; and two Qualcomm Innovation Fellowships.

References

[1] A. Sabharwal, P. Schniter, D. Guo, D. Bliss, S. Rangarajan, and R. Wichman, "In-band full-duplex wireless: Challenges and opportunities," *IEEE J. Sel. Areas Commun*, vol. 32, no. 9, pp. 1637–1652, 2014.

[2] D. Bharadia, E. McMilin, and S. Katti, "Full duplex radios," in *Proc. Association for Computing Machinery Special Interest Group on Data Communications'13*, vol. 83, no. 4, pp. 375–386, 2013.

[3] J. Marašević, J. Zhou, H. Krishnaswamy, Y. Zhong, and G. Zussman, "Resource allocation and rate gains in practical full-duplex systems," *IEEE/ACM Trans. Netw.*, vol. 25, no. 1, pp. 292–305, 2017.

[4] T. Chen, J. Diakonikolas, J. Ghaderi, and G. Zussman, "Hybrid scheduling in heterogeneous half- and full-duplex wireless networks," in *Proc. IEEE 2018 Int. Conf. Computer Communications* (*INFOCOM)*, Apr. 2018, pp. 576–584.

[5] D. Kim, H. Lee, and D. Hong, "A survey of in-band full-duplex transmission: From the perspective of PHY and MAC layers," *IEEE Commun. Surveys Tuts.*, vol. 17, no. 4, pp. 2017–2046, 2015.

[6] D. Korpi et al., "Full-duplex mobile device: Pushing the limits," *IEEE Commun. Mag.*, vol. 54, no. 9, pp. 80–87, 2016.

[7] X. Du, J. Tadrous, and A. Sabharwal, "Sequential beamforming for multiuser MIMO with full-duplex training," *IEEE Trans. Wireless Commun.*, vol. 15, no. 12, pp. 8551–8564, 2016.

[8] J. Koh, Y. Lim, C. Chae, and J. Kang, "On the feasibility of full-duplex large-scale MIMO cellular systems," *IEEE Trans. Wireless Commun.*, vol. 17, no. 9, pp. 6231–6250, Sept. 2018.

[9] M. Chung, M. S. Sim, J. Kim, D. K. Kim, and C. b. Chae, "Prototyping real-time full duplex radios," *IEEE Commun. Mag.*, vol. 53, no. 9, pp. 56–63, 2015.

[10] M. Duarte, C. Dick, and A. Sabharwal, "Experiment-driven characterization of full-duplex wireless systems," *IEEE Trans. Wireless Commun.*, vol. 11, no. 12, pp. 4296–4307, 2012.

[11] M. Duarte et al., "Design and characterization of a full-duplex multiantenna system for WiFi networks," *IEEE Trans. Veh. Technol.*, vol. 63, no. 3, pp. 1160–1177, 2014.

[12] D. Korpi, Y. S. Choi, T. Huusari, L. Anttila, S. Talwar, and M. Valkama, "Adaptive nonlinear digital self-interference cancellation for mobile inband full-duplex radio: Algorithms and RF measurements," in *Proc. IEEE 2015 Global Communications Conference* (*GLOBECOM)*, 2015, pp. 1–7.

[13] M. S. Sim, M. Chung, D. Kim, J. Chung, D. K. Kim, and C. Chae, "Nonlinear self-interference cancellation for full-duplex radios: From link-level and system-level performance perspectives," *IEEE Commun. Mag.*, vol. 55, no. 9, pp. 158–167, 2017.

[14] B. Debaillie et al., "Analog/RF solutions enabling compact full-duplex radios," *IEEE J. Sel. Areas Commun.*, vol. 32, no. 9, pp. 1662–1673, 2014.

[15] J. Zhou et al., "Integrated full duplex radios," *IEEE Commun. Mag.*, vol. 55, no. 4, pp. 142–151, 2017.

[16] D. Yang, H. Yuksel, and A. Molnar, "A wideband highly integrated and widely tunable transceiver for in-band full-duplex communication," *IEEE J. Solid-State Circuits*, vol. 50, no. 5, pp. 1189–1202, 2015.

[17] D. J. van den Broek, E. A. M. Klumperink, and B. Nauta, "An in-band full-duplex radio receiver with a passive vector modulator downmixer for self-interference cancellation," *IEEE J. Solid-State Circuits*, vol. 50, no. 12, pp. 3003–3014, 2015.

[18] T. Dinc, A. Chakrabarti, and H. Krishnaswamy, "A 60GHz CMOS full-duplex transceiver and link with polarization-based antenna and RF cancellation," *IEEE J. Solid-State Circuits*, vol. 51, no. 5, pp. 1125–1140, 2016.

[19] N. Reiskarimian, J. Zhou, and H. Krishnaswamy, "A CMOS passive LPTV nonmagnetic circulator and its application in a full-duplex receiver," *IEEE J. Solid-State Circuits*, vol. 52, no. 5, pp. 1358–1372, 2017.

[20] N. Reiskarimian, M. B. Dastjerdi, J. Zhou, and H. Krishnaswamy, "Analysis and design of commutation-based circulator-receivers for integrated full-duplex wireless," *IEEE J. Solid-State Circuits*, vol. 53, no. 8, pp. 2190–2201, 2018.

[21] T. Zhang, A. Najafi, C. Su, and J. C. Rudell, "A 1.7-to-2.2GHz full-duplex transceiver system with >50dB self-interference cancellation over 42MHz bandwidth," in *Proc. IEEE 2017 Int. Solid-State Circuits Conference (ISSCC), Feb.* 2017, pp. 314–315.

[22] S. Ramakrishnan, L. Calderin, A. Niknejad, and B. Nikolic, "An FD/FDD transceiver with RX band thermal, quantization, and phase noise rejection and >64dB TX signal cancellation," in *Proc. 2017 IEEE Radio Frequency Integrated Circuits (RFIC) Symp., June 2017, pp. 352–355.*

[23] E. Kargaran, S. Tijani, G. Pini, D. Manstretta, and R. Castello, "Low power wideband receiver with RF self-interference cancellation for full-duplex and FDD wireless diversity," in *Proc. IEEE 2017 Radio Frequency Integrated Circuits (RFIC) Symp.*, June 2017, pp. 348–351.

[24] T. Chi, J. S. Park, S. Li, and H. Wang, "A 64GHz full-duplex transceiver front-end with an on-chip multifeed self-interference-canceling antenna and an all-passive canceler supporting 4Gb/s modulation in one antenna footprint," in *Proc. IEEE 2018 Int. Solid-State Circuits Conf. (ISSCC)*, Feb. 2018, pp. 76–78.

[25] K. D. Chu, M. Katanbaf, T. Zhang, C. Su, and J. C. Rudell, "A broadband and deep-TX self-interference cancellation technique for full-duplex and frequency-domain-duplex transceiver applications," in *Proc. IEEE 2018 Int. Solid-State Circuits Conf. (ISSCC)*, Feb. 2018, 170–172.

[26] N. Reiskarimian and H. Krishnaswamy, "Magnetic-free non-reciprocity based on staggered commutation," in *Nature Commun.*, vol. 7, no. 4, p. 11217, 2016.

[27] T. Dinc and H. Krishnaswamy, "A 28GHz magnetic-free non-reciprocal passive CMOS circulator based on spatio-temporal conductance modulation," in *Proc. IEEE 2017 Int. Solid-State Circuits Conf. (ISSCC)*, Feb. 2017, pp. 294–295.

[28] M. Mikhemar, H. Darabi, and A. A. Abidi, "A multiband RF antenna duplexer on CMOS: Design and performance," *IEEE J. Solid-State Circuits*, vol. 48, no. 9, pp. 2067–2077, 2013.

[29] S. H. Abdelhalem, P. S. Gudem, and L. E. Larson, "Hybrid transformer-based tunable differential duplexer in a 90-nm CMOS process," *IEEE Trans. Microw. Theory Tech.*, vol. 61, no. 3, pp. 1316–1326, 2013.

[30] B. van Liempd et al., "A +70-dBm IIP3 electrical-balance duplexer for highly integrated tunable front-ends," *IEEE Trans. Microw. Theory Tech.*, vol. 64, no. 12, pp. 4274–4286, 2016.

[31] B. Hershberg, B. van Liempd, X. Zhang, P. Wambacq, and J. Craninckx, "A dual-frequency 0.7-to-1GHz balance network for electrical balance duplexers," in *Proc. IEEE 2016 Int. Solid-State Circuits Conf. (ISSCC)*, Jan. 2016, pp. 356–357.

[32] H. Nawaz and I. Tekin, "Double-differential-fed, dual-polarized patch antenna with 90 dB interport RF isolation for a 2.4 GHz in-band full-duplex transceiver," *IEEE Antennas Wireless Propag. Lett.*, vol. 17, no. 2, pp. 287–290, 2018.

[33] J. Zhou, T. H. Chuang, T. Dinc, and H. Krishnaswamy, "Integrated wideband self-interference cancellation in the RF domain for FDD and full-duplex wireless," *IEEE J. Solid-State Circuits*, vol. 50, no. 12, pp. 3015–3031, 2015.

[34] A. Sahai, G. Patel, C. Dick, and A. Sabharwal, "On the impact of phase noise on active cancelation in wireless full-duplex," *IEEE Trans. Veh. Technol.*, vol. 62, no. 9, pp. 4494–4510, 2013.

[35] D. J. van den Broek, E. A. M. Klumperink, and B. Nauta, "A self-interference cancelling front-end for in-band full-duplex wireless and its phase noise performance," in *Proc. IEEE 2015 Radio Frequency Integrated Circuits (RFIC) Symp.)*, May 2015, pp. 75–78.

[36] Y.-S. Choi and H. Shirani-Mehr, "Simultaneous transmission and reception: Algorithm, design and system level performance," *IEEE Trans. Wireless Commun.*, vol. 12, no. 12, pp. 5992–6010, 2013.

[37] J. I. Choi, M. Jain, K. Srinivasan, P. Levis, and S. Katti, "Achieving single channel, full duplex wireless communication," in *Proc. 16th Annu. Int. Conf. on Mobile Computing and Networking*, 2010, pp. 1–12.

[38] M. Heino, S. N. Venkatasubramanian, C. Icheln, and K. Haneda, "Design of wavetraps for isolation improvement in compact in-band full-duplex relay antennas," *IEEE Trans. Antennas Propag.*, vol. 64, no. 3, pp. 1061–1070, 2016.

[39] K. Iwamoto, M. Heino, K. Haneda, and H. Morikawa, "Design of an antenna decoupling structure for an inband full-duplex collinear dipole array," *IEEE Trans. Antennas Propag.*, vol. 66, no. 7, pp. 3763–3768, 2018.

[40] M. Duarte, C. Dick, and A. Sabharwal, "Experiment-driven characterization of full-duplex wireless systems," *IEEE Trans. Wireless Commun.*, vol. 11, no. 12, pp. 4296–4307, 2012.

[41] S. Tanaka, N. Shimomura, and K. Ohtake, "Active circulators - the realization of circulators using transistors," *Proc. IEEE*, vol. 53, no. 3, pp. 260–267, 1965.

[42] N. A. Estep, D. L. Sounas, J. Soric, and A. Alu, "Magnetic-free non-reciprocity and isolation based on parametrically modulated coupled-resonator loops," *Nature Physics*, vol. 10, no. 12, pp. 923–927, 2014.

[43] N. A. Estep, D. L. Sounas, and A. Alu, "Magnetless microwave circulators based on spatiotemporally modulated rings of coupled resonators," *IEEE Trans. Microw. Theory Techn.*, vol. 64, no. 2, pp. 502–518, 2016.

[44] S. Qin, Q. Xu, and Y. E. Wang, "Nonreciprocal components with distributedly modulated capacitors," *IEEE Trans. Microw. Theory Techn.*, vol. 62, no. 10, pp. 2260–2272, 2014.

[45] T. Dinc, M. Tymchenko, A. Nagulu, D. Sounas, A. Alu, and H. Krishnaswamy, "Synchronized conductivity modulation to realize broadband lossless magnetic-free non-reciprocity," *Nature Commun.*, vol. 8, no. 1, p. 795, 2017.

[46] A. Ghaffari, E. A. M. Klumperink, M. C. M. Soer, and B. Nauta, "Tunable high-Q N-path band-pass filters: Modeling and verification," *IEEE J. Solid-State Circuits*, vol. 46, no. 5, pp. 998–1010, 2011.

[47] A. Nagulu, A. Alù, and H. Krishnaswamy, "Fully-integrated non-magnetic 180nm SOI circulator with >1W P1dB, >+50dBm IIP3 and high isolation across 1.85 VSWR," in *Proc. IEEE 2018 Radio Frequency Integrated Circuits (RFIC) Symp.*, 2018.

[48] S. Jayasuriya, D. Yang, and A. Molnar, "A baseband technique for automated LO leakage suppression achieving <80dBm in wideband passive mixer-first receivers," in *Proc. IEEE 2014 Custom Integrated Circuits Conf.*, Sept. 2014, pp. 1–4.

[49] N. Reiskarimian, A. Nagulu, T. Dinc, and H. Krishnaswamy, "Integrated conductivity-modulation-based RF magnetic-free non-reciprocal components: Recent results and benchmarking," *IEEE Antennas Wireless Propag. Lett.*, vol. 17, Nov. 2018, pp. 1978–1982.

[50] T. Chen et al., "Demo: Full-duplex wireless based on a small-form-factor analog self-interference canceller," in *Proc. IEEE Seventeenth Int. Symp. Mobile Ad Hoc Networking and Computing*, 2016, pp. 367–358.

[51] T. Chen et al., "Demo abstract: Full-duplex with a compact frequency domain equalization-based RF canceller," in *Proc. IEEE 2018 Int. Conf. Computer Communications (INFOCOM)*, 2017, pp. 972–973.

[52] T. Chen, M. B. Dastjerdi, G. Farkash, J. Zhou, H. Krishnaswamy, and G. Zussman, Open-access full-duplex wireless in the orbit testbed. 2018. [Online]. Available: arXiv:1801.03069v2.

[53] T. Chen, M. B. Dastjerdi, J. Zhou, H. Krishnaswamy, and G. Zussman, "Wideband full-duplex wireless via frequency-domain equalization: Design and experimentation," in *Proc. 25th Annu. Int. Conf. Mobile Computing and Networking*, 2019.

[54] M. B. Dastjerdi, N. Reiskarimian, T. Chen, G. Zussman, and H. Krishnaswamy, "Full duplex circulator-receiver phased array employing self-interference cancellation via beamforming," in *Proc. IEEE Radio Frequency Integrated Circuits Symp. (RFIC)*, 2018, pp. 108–111.

[55] M. B. Dastjerdi, S. Jain, N. Reiskarimian, A. Natarajan, and H. Krishnaswamy, "Full-duplex 2×2 MIMO circulator-receiver with high TX power handling exploiting MIMO RF and shared-delay baseband self-interference cancellation," in Proc. *ISSCC. 2019 IEEE Solid-State Circuits Conf.*, to be published.